

SCHEME: Scalable Channer Mixer for Vision Transformers

Deepak Sridhar¹, Yunsheng Li², and Nuno Vasconcelos¹
{desridha,nvasconcelos}@ucsd.edu, yunshengli@microsoft.com

¹University of California, San Diego, ²Microsoft

Abstract. Vision Transformers have received significant attention due to their impressive performance in many vision tasks. While the token mixer or attention block has been studied in great detail, the channel mixer or feature mixing block (FFN or MLP) has not been explored in depth albeit it accounts for a bulk of the parameters and computation in a model. In this work, we study whether sparse feature mixing can replace the dense connections and confirm this with a block diagonal MLP structure that improves the accuracy by supporting larger expansion ratios. To improve the feature clusters formed by this structure and thereby further improve the accuracy, a lightweight, parameter-free, channel covariance attention (CCA) mechanism is introduced as a parallel branch during training. This design of CCA enables gradual feature mixing across channel groups during training whose contribution decays to zero as the training progresses to convergence. This allows the CCA block to be discarded during inference, thus enabling enhanced performance with no additional computational cost. The resulting *Scalable CHannel MixEr* (SCHEME) can be plugged into any ViT architecture to obtain a gamut of models with different trade-offs between complexity and performance by controlling the block diagonal structure size in the MLP. This is shown by the introduction of a new family of SCHEMEformer models. Experiments on image classification, object detection, and semantic segmentation, with different ViT backbones, consistently demonstrate substantial accuracy gains over existing designs, especially under lower FLOPs regimes. The SCHEMEformer family is shown to establish new Pareto frontiers for accuracy vs FLOPS, accuracy vs model size, and accuracy vs throughput, especially for fast transformers of small model size.

1 Introduction

Vision Transformers (ViTs) [14, 30, 31, 46] have become ubiquitous in computer vision in recent years. Under this architecture, an image is decomposed into a set of patches which are considered as tokens and fed to a transformer model [45] of two main components: a *spatial attention* module, which reweighs each token according to its similarity to the other tokens extracted from the image, enabling information fusion across large spatial distances, and a *channel mixer* that combines the feature channels extracted from all patches using a multi-layer perceptron (MLP or FFN). A bottleneck of this model is the quadratic complexity of the attention mechanism on the number of patches. Numerous ViT variants have been proposed in recent years to improve complexity and/or

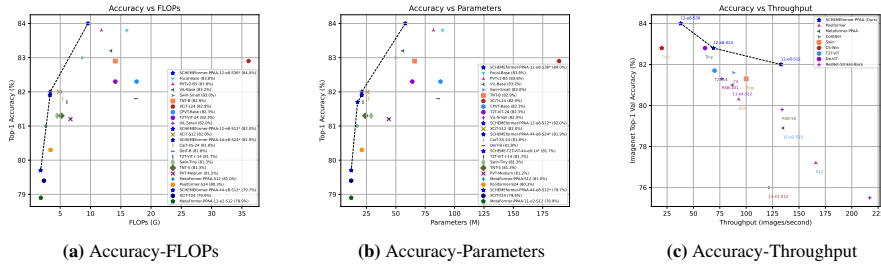


Fig. 1: Comparison of the proposed SCHEMEformer family, derived from the Metaformer-PPAA-S12 model [55] with higher expansion ratios in the MLP blocks, and many SOTA transformers from the literature. The SCHEMEformer family establishes a new Pareto frontier (optimal trade-off) for a) accuracy vs. FLOPs, b) accuracy vs model size, and c) accuracy vs. throughput. SCHEMEformer models are particularly effective for the design of fast transformers (throughput between 75 and 150 images/s) with small model size.

accuracy. These can be grouped into 1) improved attention mechanisms, and 2) hybrid architectures that replace attention or combine it with convolutions. Much less research has been devoted to the channel mixer. Most models simply adopt the MLP block of [45], consisting of two layers, where channels are first expanded by a specified *expansion ratio* and then compressed to the original dimension. This is somewhat surprising since the mixer is critical for good transformer performance. For example, [13] showed that pure attention, without MLPs or residual connections, collapses doubly exponentially to a rank one matrix. [55] also showed that without residual connections or MLP, the model cannot converge. [11] showed that replacing MLPs with more attention blocks (both spatial and channel attention) of equivalent computational complexity lowers the transformer accuracy. These observations show that the channel mixer is an indispensable component of ViTs.

In this work, we investigate the channel mixer module, both to quantify its contribution to ViT performance and to improve the complexity vs. accuracy trade-off of the transformer model. We show that enhanced design of the channel mixer can lead to significant improvements in transformer performance by introducing a novel *Scalable CHannel MixEr* (SCHEME) that enables the design of models with larger expansion ratios. SCHEME is a generic channel mixer that can be plugged into existing ViT variants to obtain effective scaled-down or scaled-up model versions. We replace the channel mixer of the MetaFormer-PPAA-S12 [55] model with SCHEME to obtain a new family of **SCHEMEformer** models with improved accuracy/complexity trade-off. This is shown in Figure 1, where the SCHEMEformer family establishes new Pareto frontiers for accuracy vs FLOPs, accuracy vs model size, and accuracy vs throughput, showing that SCHEME allows fine control over all these variables, while guaranteeing SOTA performance. These properties are shown to hold for image classification, object detection and semantic segmentation tasks, as well as for different architectures, such as T2T-ViT [57], CoAtNet [8], Swin Transformer [30], CSWin [12] and DaViT [11].

To develop SCHEME, we start by studying the impact of the channel expansion performed in the mixer, by varying its expansion ratio. Transformer performance is shown to increase until it saturates for an expansion ratio beyond 8. However, because mixer (MLP) complexity is linear on the dimension of the intermediate representation, naive

channel scaling with expansion ratios larger than 4 causes an explosion of parameters and computation, leading to models of large complexity and prone to overfit. To achieve a better trade-off between dimensionality and computation, we seek to leverage a hardware efficient mixer with block diagonal structure [1, 9]. This consists of breaking the input and output feature vectors of a network layer into disjoint groups and performing matrix multiplications only within each group, as illustrated in Figure 2. We denote the resulting MLP block as *Block Diagonal MLP* (BD-MLP). Despite the lack of feature mixing across groups, we find that a transformer model equipped with the BD-MLP and a larger expansion ratio (to match both the parameter count and computation) achieves comparable or slightly higher accuracy than a baseline with the dense MLP. This suggests that the lower accuracy of the sparse block diagonal operations is offset by the gains of larger expansion ratios. Further analyzing the features learned by the different groups of the BD-MLP, we observe that they form feature clusters that are similar in terms of their discriminative ability to identify the target classes. To learn better feature clusters, we seek a mechanism capable of restoring inter-group feature communication only during training without increasing parameters. For this, we propose to use the channel correlations among features. This is done by introducing a channel attention branch that computes the channel covariance matrix of the input features of the BD-MLP and is used to re-weigh its output features, as illustrated in Figure 2. This attention mechanism is denoted as the *channel covariance attention* (CCA) block. The reweighted features are then fused with the BD-MLP output by means of a weighted residual addition with learned weights $(\alpha, 1 - \alpha)$.

As shown in Figure 2, SCHEME combines the sparse block diagonal structure of the BD-MLP, and the parameter-free CCA attention module, to implement a channel mixer extremely efficient in terms of parameters. Experiments also show that the fusion weight learned in the CCA branch, denoted as $1 - \alpha$ in Fig. 2, gradually decays to zero during training. This happens consistently across all layers of the model and across model architectures. While the CCA is important for the formation of good feature clusters during training, it can be removed at inference without any loss, as illustrated in Figure 2. As a result, the model accuracy improves over simply using the BD-MLP mixer, but the computational complexity of model inference does not. This leads to an extremely efficient inference setup, both in terms of parameters and FLOPs. We empirically verify the hypothesis through ablations that study the evolution of attention branch weights over training and the class separability of the learned feature groups.

Overall, the paper makes the following contributions,

- a study of the channel mixer of ViT MLPs, showing that dense feature mixing can be replaced by sparse feature mixing of higher internal feature dimensionality for improved accuracy, without increased complexity.
- the SCHEME module, which combines 1) a BD-MLP to enable internal feature representations of larger dimensionality than previous MLP blocks, and 2) CCA to enable the learning of these representations without cost at inference.
- various models that combine SCHEME with previous transformer architectures to achieve SOTA trade-offs between accuracy and model size, FLOPs, or throughput, such as the SCHEMEformer of Figure 1. This is shown particularly effective for the design of fast transformers with small model size, of interest for edge devices, robotics, and low-power applications.

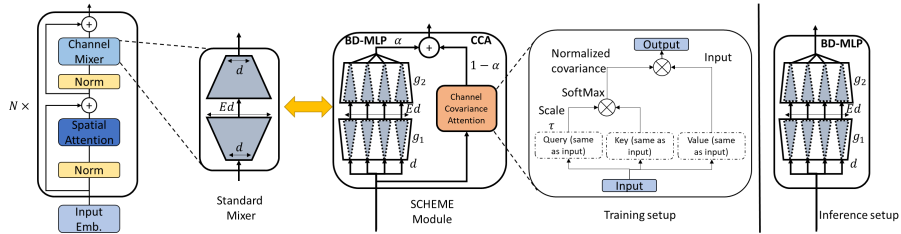


Fig. 2: Proposed SCHEME channel mixer. The channel mixer of the standard transformer consists of two MLP layers, performing dimensionality expansion and reduction by a factor of E . SCHEME uses a combination of a block diagonal MLP (BD-MLP), which reduces the complexity of the MLP layers by using block diagonal weights, and a channel covariance attention (CCA) mechanism that enables communication across feature groups through feature-based attention. This, however, is only needed for training. The weights $1 - \alpha$ decay to zero upon training convergence and CCA can be discarded during inference, as shown on the right. Experiments show that CCA helps learn better feature clusters, but is not needed once these are formed.

- Experiments on image classification, object detection, and semantic segmentation, showing consistent gains in accuracy for fixed computation and model size.

2 Related Work

Vision Transformers: Vision transformers advanced the state-of-the-art in several vision tasks since [14, 31] successfully applied the transformer-based self-attention NLP model of [45] to image generation and classification tasks. These models rely on a spatial attention mechanism, based on the matrix of dot-products between features extracted from image patches. This has quadratic complexity in the number of patches and is quite intensive. Most follow up work [18, 37–39, 42, 44, 50, 56–58] improved the spatial attention mechanism of ViT. DeiT [39] and subsequent works [40, 41] introduced a distillation token to distill information, typically from a CNN teacher, without large amounts of data or compute. PvT [46] proposed a progressive shrinking pyramid architecture with spatial-reduction attention that scales ViTs for dense prediction tasks beyond image classification. Swin transformers [30] introduced a hierarchical shifted window attention mechanism, which reduces the complexity to linear with respect to the number of windows. HaloNet [44] proposed two extensions for local ViTs [32] with blocked local attention and relaxed translational equivariance for scaling ViTs. A more extensive review of ViTs is given in [29].

Recently, several works have shown that spatial attention is not the critical ViT feature. Some works improved performance by relying on hybrid architectures, which augment or replace ViT layers with convolutions [43, 49]. Efficient transformer designs, for edge devices, frequently sacrifice spatial attention to achieve better trade-offs between FLOPs and accuracy [4, 24]. Other works have questioned the need for spatial attention altogether. Metaformer [55] argued that the fundamental trait of ViT is the mixing of information across patches, showing that competitive results can be obtained by simply replacing attention with pooling or identity operations. Similarly, [28] showed that spatial attention is not critical for vision transformers by proposing a spatial-gating MLP of comparable performance to ViT [14]. DaViT [11] showed that it is helpful by

Table 1: Effect of the MLP block expansion ratio (E) on ImageNet-1K validation accuracy for the MetaFormer-S12 [55] architecture. * denotes results obtained with the code made publicly available by the authors.

Model	Expansion ratio (E)	FLOPs (G)	Top-1 Acc (%)
Metaformer-PPAA-S12*	8	4.14	81.6 (+0.6)
Metaformer-PPAA-S12*	6	3.35	81.8 (+0.8)
Metaformer-PPAA-S12 [55]	4	2.55	81.0 (+0.0)
Metaformer-PPAA-S12*	2	1.77	78.9 (-2.1)
Metaformer-PPAA-S12*	1	1.33	76.0 (-5.0)
Metaformer-PPAA-S18*	1	2.51	78.3 (-2.7)

simply reusing the spatial attention design for channel attention, building a cascade of alternating spatial and channel attention blocks. While this improves performance, it increases the complexity of the transformer block, resulting in a model with many parameters and potentially redundant channel mixer operations. Despite all this work on ViT architectures, little emphasis has been devoted to the other main component of the transformer: the channel mixer module (MLP) that follows attention. This is surprising because the mixer dominates both the parameter count and complexity (FLOPs) of the standard transformer block. [25, 56] modify the MLP block to mimic the inverted residual block of the MobileNetV2 [34], by adding a depthwise convolution. This improved performance but increases parameter and computation costs. Switch Transformer [16] replaces the FFN with sparse mixture of experts [36] that dynamically routes the input tokens. This design allows scaling models to large sizes using higher number of experts, however its not effective for ViTs. In this work, we instead propose an efficient and generic channel mixer module that improves both the parameter and computational efficiency of the transformer and allows for flexible scaling of ViTs.

3 The SCHEME module

Figure 2 depicts the proposed SCHEME module for feature mixing in ViTs. As shown on the left, the standard channel mixer consists of two MLP layers, which expand the dimensionality of the input features and then reduce it to the original size. Let $\mathbf{x} \in \mathbb{R}^{d \times N}$ be the matrix containing the N d -dimensional input feature vectors extracted from N image patches. The mixer computes an intermediate representation $\mathbf{z} \in \mathbb{R}^{Ed \times N}$ and an output representation $\mathbf{y} \in \mathbb{R}^{d \times N}$ according to

$$\mathbf{z} = \sigma(\mathbf{W}_1 \mathbf{x} + \mathbf{b}_1 \mathbf{1}_N^T) \quad (1)$$

$$\mathbf{y} = \mathbf{W}_2 \mathbf{z} + \mathbf{b}_2 \mathbf{1}_N^T \quad (2)$$

where $\mathbf{W}_1 \in \mathbb{R}^{Ed \times N}$, $\mathbf{W}_2 \in \mathbb{R}^{d \times Ed}$, $\mathbf{b}_1 \in \mathbb{R}^{Ed}$, $\mathbf{b}_2 \in \mathbb{R}^d$, $\mathbf{1}_N$ is the N -dimensional vector containing ones as all entries, $\sigma(\cdot)$ is the activation function (typically GELU), and E is an expansion factor, typically 4.

Table 1 details the impact of the mixer on overall transformer performance by evaluating the role of the expansion factor E on the performance of MetaFormer-PPAA-S12 [55] (Pooling, Pooling, Attention, Attention) architecture on ImageNet-1K. Classification accuracy increases from 76.0 to 81.8%, as E ranges from 1 to 6, decreasing for $E = 8$, which suggests overfitting. The table also shows that these gains are not trivial. The S18 model, which has no expansion ($E = 1$) but more transformer layers

and complexity comparable to that of the S12 model with $E = 4$, has an accuracy 2.7 points lower than the latter. In summary, for a given computation budget, it is beneficial to trade off transformer depth for dimensionality expansion in the channel mixer. This shows that this expansion is a critical component of the transformer architecture. On the other hand, naively scaling E beyond 6 severely increases parameters and computation, leading to models that over-fit and are impractical for many applications.

3.1 Scalable Channel Mixer (SCHEME)

To efficiently realize the gains of higher intermediate MLP feature dimensionality, we propose the SCHEME module, which consists of a BD-MLP and CCA block where the CCA branch is only used during training. These are now discussed.

Block Diagonal MLP (BD-MLP): Block diagonal matrices have been previously proposed to efficiently approximate dense matrices [1, 9]. In CNNs, group channel operations are frequently used to design lightweight mobile models with improved accuracy-computation trade-off [5, 23, 34]. This consists of splitting the feature vectors of (1)-(2) into disjoint groups, e.g. \mathbf{x} into a set of g_1 disjoint features $\{\mathbf{x}_k\}_{k=1}^{g_1}$ where $\mathbf{x}_k \in \mathbb{R}^{d/g_1 \times N}$, and \mathbf{y} into a set $\{\mathbf{y}_k\}_{k=1}^{g_2}$ where $\mathbf{y}_k \in \mathbb{R}^{Ed/g_2 \times N}$. As illustrated in Figure 2, the MLPs of (1)-(2) are then implemented independently for each group, according to

$$\mathbf{z}_k = \sigma(\mathbf{W}_{1,k}\mathbf{x}_k + \mathbf{b}_{1,k}\mathbf{1}_N^T) \quad (3)$$

$$\mathbf{y}_k = \mathbf{W}_{2,k}\mathbf{z}_k + \mathbf{b}_{2,k}\mathbf{1}_N^T \quad (4)$$

where $\mathbf{W}_{1,k} \in \mathbb{R}^{Ed/g_1 \times N/g_1}$, $\mathbf{W}_{2,k} \in \mathbb{R}^{d/g_2 \times Ed/g_2}$, $\mathbf{b}_{1,k} \in \mathbb{R}^{Ed/g_1}$, $\mathbf{b}_{2,k} \in \mathbb{R}^{d/g_2}$ and \mathbf{z} is decomposed into a set $\{\mathbf{z}_k\}_{k=1}^G$ where $\mathbf{z}_k \in \mathbb{R}^{Ed/G \times N}$, with $G = g_1$ in (3) and $G = g_2$ in (4). Since the complexity of (3) is g_1^2 times smaller than that of (1) and there are g_1 groups, the complexity of the first MLP is $1/g_1$ times that of standard MLP. Similarly, the complexity of the second MLP is $1/g_2$ times that of the standard MLP. Hence, a transformer equipped with the BD-MLP and expansion factor $\frac{2g_1g_2}{g_1+g_2}E$ has identical complexity to a standard transformer of factor E . For example, when $g_1 = g_2 = g$ this allows growing the expansion factor by a factor of g without computational increase.

Channel Covariance Attention (CCA): While the introduction of groups enables accuracy gains due to the increased expansion factor by $\frac{2g_1g_2}{g_1+g_2}$, it results in sub-optimal features. This is because the features in the different groups of (3)-(4) are processed *independently*, i.e. there is no inter-group feature fusion. This reduces the efficiency of the BD-MLP. To enable feature mixing between *all* feature channels and thus induce the formation of better feature clusters, we introduce a covariance attention mechanism in a parallel branch, as illustrated in Figure 2. The input features are first transposed to obtain the $d \times d$ covariance matrix¹ $\mathbf{x}\mathbf{x}^T$. This is then used to re-weigh the input features by their covariance with other feature channels, using

$$CCA(\mathbf{x}) = \text{softmax}\left(\frac{\mathbf{x}\mathbf{x}^T}{\tau}\right)\mathbf{x} \quad (5)$$

¹ Since the features are normalized before the mixer, i.e centered such that $\mathbf{x}\mathbf{1}_N = 0$, $\mathbf{x}\mathbf{x}^T$ is the covariance matrix of features \mathbf{x} .

Table 2: Scaling MetaFormer-PPAA using SCHEME. Each column of the table reports to one baseline model (S12 to S36) of increasing size. P and F denote Parameters and FLOPs respectively. SCHEMEformer-PPAA-44-e8 (SCHEMEformer-PPAA-12-e8) models use configurations g_1 , g_2 , and E that downscale (upscale) the baseline.

Model	S12		S24		S36	
	P (M)	F (G)	P (M)	F (G)	P (M)	F (G)
SCHEMEformer-PPAA-44-e8	12	1.8	21	3.3	55	7.96
SCHEMEformer-PPAA-12-e8	21	3.3	40	6.5	59	9.6

where the softmax operation is applied across the matrix rows and τ is a smoothing factor. The output of the channel mixer block is obtained by the weighted summation of the BD-MLP and CCA branches, according to

$$\mathbf{y}_{out} = \alpha \mathbf{y} + (1 - \alpha) CCA(\mathbf{x}) \quad (6)$$

where α is a mixing weight learned across all samples. Various other design choices are discussed in Section 4.2.

CCA as a Regularizer: The introduction of a parameter free attention branch and a learnable weight α allows the model to form better feature clusters during training and gradually decay the contribution from CCA branch once the feature clusters are formed. This can be seen in Figure 4a, which plots the value of the learned mixing weight $1 - \alpha$ as a function of training epochs on ImageNet-1K, for all transformer layers. These plots are typical of the behavior we observed with all transformer backbones and architectures we considered. Clearly, $1 - \alpha$ starts with high to intermediate values, indicating that information flows through both branches of the mixer, but decays to $1 - \alpha \approx 0$ as training converges. Hence, there is no degradation if the CCA branch is removed during inference. This eliminates a substantial amount of computation during inference, leading to the the training and inference setup of Figure 2, where CCA is not used at inference.

We explain this behavior by conjecturing that the downside of the computational efficiency of the BD-MLP is a more difficult learning problem, due to the independent processing of channel groups. This creates symmetries in the cost function, e.g. the order of the feature groups is not important, and requires a feature clustering operation that is likely to produce more local minima. The CCA branch helps to smooth out this cost function during training, while the feature groups are not established, by allowing inter-group communication. However, once the right feature groupings are found, CCA is no longer needed, and a simple BD-MLP mixer has no loss of performance over the standard MLP. Note that the operation of (5) is basically a projection of \mathbf{x} into canonical subspaces of features that are correlated in the input image. This is likely to be informative to guide the group formation, but less useful when the features are already clustered. While this hypothesis is not trivial to test, since (5) varies from example to example, we confirmed that using CCA during training enhances class separability, which likely reduces overfitting for large expansion ratios. See the results section for more details.

3.2 The SCHEMEformer family

The proposed SCHEME module enables efficient control of model complexity via the mixer hyperparameters g_1 , g_2 , and E . Table 1 shows that naively scaling down the ViT model by simply reducing E causes a significant accuracy loss. The SCHEME module allows much more effective control of the accuracy/complexity trade-off, producing models of better performance for a fixed computational budget. This is demonstrated by the introduction of a new family of models, denoted as SCHEMEformer, obtained by replacing the channel mixer of the Metaformer-PPAA [55] architecture with the SCHEME module. Two such configurations are shown in Table 2 where the naming follows the convention {model-name}-{ g_1 g_2 }-e{ E }. These are shown to achieve SOTA accuracy for lower computational budgets in the experiments section, where we also discuss results with other backbones.

3.3 Computational Complexity

The complexity of the BD-MLP block is controlled by the group numbers g_1 , g_2 and the expansion factor E , with a total cost $\mathcal{O}(Ed^2/g_1 + Ed^2/g_2)$, where d is the channel dimension. The computational cost of CCA is $\mathcal{O}(Nd^2)$ where N is the number of tokens. Since CCA is not used during inference, it only adds to the computations during training. The SCHEME framework provides a systematic way to control the trade-off of transformer width vs depth, by controlling the block size and expansion hyperparameters.

4 Experimental Results

In this section, we discuss an evaluation of the SCHEME module on Image Classification (ImageNet-1K [10]), Object Detection (COCO-17 [27]), and Semantic Segmentation (ADE-20K [61]) benchmarks.

4.1 Comparisons to the state of the art

Implementation Details: For image classification, we use a batch size of 1024, adjusted according to memory availability, and train all models on 8 GPUs with AdamW optimizer and cosine annealing learning rate schedule, of learning rate $1e-3$. Warmup learning is applied in the first 5 epochs. Object detection is based on the setting of [55], where all backbones are trained with RetinaNet [26] and Mask-RCNN [19] detection heads, for a fair comparison with prior methods. A 1x learning schedule (12 epochs with AdamW optimizer and initial learning rate of $1e-4$) is used and all models are implemented with the mmdetection [2] codebase, capping input sizes at 800, 1333 for the shorter and longer sides, respectively. For semantic segmentation, following prior methods [3, 22, 55], we train with a batch size of 16 for 80,000 iterations with AdamW optimizer and an initial learning rate of $2e-4$. We use the mmsegmentation [7] codebase with an input size 512×512 for training and resize the shorter side to 512 pixels for testing. For both detection and segmentation, imagenet pretrained models are used to initialize the backbones.

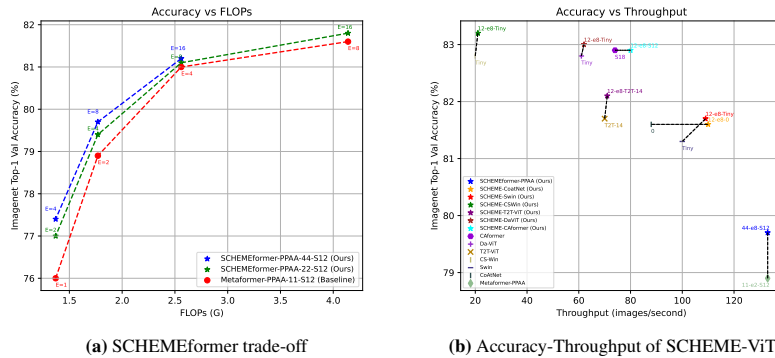


Fig. 3: Performance of various SCHEME models obtained by replacing the MLP blocks in popular ViT architectures. SCHEME mixer improves the accuracy for a fixed throughput or improves the throughput for the same accuracy.

Image Classification: Image classification is evaluated on Imagenet-1K, without using extra data. We report the results with single crop top-1 accuracy at 224×224 input resolution. We evaluate the SCHEMEformer family of models based on the Metaformer-PPAA-S12 [55] obtained by replacing the MLP of the latter with the SCHEME module.

We start by evaluating how this improves the trade-off between model accuracy and complexity. Figure 3 a) compares the performance of the Metaformer-PPAA-S12 with expansion ratios $E \in \{1, 2, 4, 8\}$ to comparable variants of the SCHEMEformer-PPAA-S12, with SCHEME mixers of either $g = 2$ (green curve) or $g = 4$ (blue curve) groups. It can be seen that the SCHEMEformer models have a better trade-off between accuracy and FLOPs, achieving higher accuracies for all complexity levels. Among the two SCHEMEformer models, the one with more feature groups ($g = 4$) has the best performance. As discussed in Section 3.1, when $g_1 = g_2$, a SCHEME transformer of expansion factor gE has identical complexity to a standard transformer of expansion factor E . Hence, for fixed FLOPs, SCHEME allows an increase of the expansion factor by g . Figure 3 a) shows that this is beneficial at all FLOP levels, but has larger gains for lower complexity models. This makes SCHEME particularly attractive for the design of low complexity transformers, e.g. for edge devices or equivalent applications.

We next compare the SCHEMEformer family against the SOTA transformers in the literature. This is not an easy comparison, since models vary in size, FLOPs, and throughput. Because it is difficult to make any of these variables exactly the same for two different architectures, the comparison is only possible in terms of how the different architectures trade-off accuracy for any of the other factors. For a given pair of variables, e.g. FLOPs vs accuracy, the model is said to be on the Pareto frontier of the two variables if it achieves the best trade-off between the two. This is usually best understood by visualizing plots of this trade-off. We use plots to make comparisons to larger numbers of baselines and tables to enable more precise comparisons with respect to a smaller number of baselines.

Table 3 presents a comparison of the SCHEMEformer family against various SOTA transformers in the literature. Each section of the table compares a SCHEMEformer model to a group of SOTA transformers of equivalent size or complexity. Note that,

Table 3: Image Classification on ImageNet-1K dataset. **Table 4: Semantic Segmentation** Comparison with SOTA ViT models grouped by the accuracy results on ADE20K dataset. FLOPs racy. Proposed SCHEME based models use an expansion ratio 8. SCHEMEformer family achieves higher throughput and accuracy compared to SOTA ViT models.

Model	#Params (M)	FLOPs (G)	Thru (im/s)	Top-1 Acc (%)
ViT-L/16 [14]	307	63.6	37	76.1
MetaFormer-PPAA-11-e2-S12 [55]	12	1.8	133	78.9
XCiT-T24 [15]	12	2.3	-	79.4
ViT-B/16 [14]	86	17.6	112	79.7
SCHEMEformer-PPAA-44-S12	12	1.77	133	79.7
MetaFormer-PPAA-S12 [55]	17	2.6	87	81.0
Swin-Tiny [30]	29	4.5	100	81.3
T2T-ViT t-14 [57]	22	6.1	70	81.7
DeiT-B [39]	86	17.5	114	81.8
ViL-Small [59]	25	5.1	-	82.0
SCHEMEformer-PPAA-12-S12	21	3.35	130	82.0
Focal-Tiny [54]	29	4.9	29	82.2
CPVT-Base [6]	88	17.6	-	82.3
DaViT-Tiny [11]	23.0	4.3	61	82.8
CSWin-Tiny [12]	23.0	4.3	20	82.8
SCHEMEformer-PPAA-12-S24	40	6.47	69	82.8
XCiT-L24 [15]	189	36.1	-	82.9
Swin-Small [30]	50	8.7	31	83.0
ViL-Base [59]	56	13.4	-	83.2
CSWin-Small [12]	35	6.9	11	83.6
SCHEMEformer-PPAA-12-S36	58	9.58	38	84.0

Backbone	#P (M)	F (G)	mIoU (%)
Semantic FPN			
PVT-Tiny [46]	17	33.2	35.7
ResNet-50 [20]	29	45.6	36.7
PoolFormer-S12 [55]	16	30.9	37.2
ResNeXt-101-32x4d [53]	47	64.7	39.7
PVT-Small [46]	28	44.5	39.8
XCiT-T12/8 [15]	8.4	-	39.9
PoolFormer-S24 [55]	23	39.3	40.3
SCHEMEformer-44-S12	15.5	34.3	40.9
PVT-Medium [46]	48	61.0	41.6
PoolFormer-S36 [55]	35	47.5	42.0
PVT-Large [46]	65	79.6	42.1
PoolFormer-M36 [55]	60	67.6	42.4
SCHEMEformer-44-S24	24.8	45.7	42.5
UperNet			
Swin-Tiny [30]	60	945	44.5
PVT-Large [47]	65	318	44.8
Focal-Tiny [54]	62	998	45.8
XCiT-S12/16 [15]	52	-	45.9
DaViT-Tiny [11]	60	940	46.3
SCHEME-DaViT-12-Tiny	68	969	47.1

in each section, the remaining models tend to be either larger in size or have lower throughput than the SCHEMEformer model but always have lower accuracy than the latter. Figure 1 provides a broader visualization of how SCHEME models establish Pareto frontiers for accuracy vs FLOPs, accuracy vs throughput, and accuracy vs model size (parameters). Figure 1 a) illustrates the trade-off between accuracy and FLOPs of many SOTA transformers. The dashed line connects the SCHEMEformer model results, summarizing the accuracy-FLOPs trade-off of the family. It can be seen that the SCHEME models lie on the Pareto frontier for these two objectives. This illustrates the fine control that SCHEME allows over the accuracy/complexity trade-off of transformer models. Figure 1 b) presents a similar comparison for model sizes. Like for FLOPs, the SCHEME models lie on the Pareto frontier for accuracy vs model size. In fact the two plots are quite similar, showing that in general there is a good correlation between model size and FLOPs.

This is not the case for throughput, which for transformers is known to not necessarily correlate with FLOPs, due to the parallelism of certain computations and the ability of GPUs to leverage that parallelism. For example, Table 3 shows that, CSWin models have lower throughput despite having lower FLOPs while ViT has higher throughput despite having higher FLOPs. SCHEMEformer controls this trade-off by controlling the expansion ratio and block diagonal structure, which enables higher FLOPs utilization for a given throughput [17]. We compute throughput on a NVIDIA-Titan-X GPU with a batch size of 1 averaged over 1000 runs. While comparisons may also be made for large batch sizes, we consider the setting of largest relevance for live/streaming applications, where speed is most critical. In these applications, the concern is usually inference throughput, which requires batch size of 1. Figure 1 c) illustrates the trade-off

between accuracy and throughput of various models, including very fast ResNet models of low accuracy. It can be seen that the SCHEMEformer again achieves the best trade-off between these two variables, thus lying on the Pareto frontier for accuracy vs throughput. Its performance is particularly dominant in the range of throughputs between 75 and 150 images/sec, where it significantly outperforms the other methods. These results demonstrate how the SCHEME module endows transformer designers with the ability to produce multiple models at different points of the Pareto frontiers of accuracy vs model size, FLOPS, or throughput.

SCHEME with other ViTs: Figure 3b shows the Accuracy-Throughput curves for various SCHEME models obtained by replacing the MLP blocks of popular ViT architectures. It shows that SCHEME improves the accuracy for a fixed throughput, the throughput for a fixed accuracy, or both. The gains can be substantial, e.g. about 1% accuracy gain (constant throughput) for the fastest transformer or speed gains of up to 20% at constant accuracy. This shows that SCHEME benefit various ViT backbones, not just the MetaFormer.

Semantic Segmentation: Table 4 compares the semantic segmentation performance of two SCHEMEformer models using the semantic FPN framework [22] to various SOTA models of similar complexity, on ADE20K. Since we do not have access to the throughput of most models, we report only parameter sizes and FLOPS. In each section of the table, the remaining models² have equivalent or larger FLOPs and model size than the SCHEMEformer. All of the models have lower accuracy than the comparable SCHEMEformer. For example, SCHEMEformer-44-e8-S12 achieves 40.9% mIoU, which is 5.2/3.7 points higher than the comparable Pvt-Tiny/PoolFormer-S12 which both have very similar size and FLOPs. Similarly, the S24 model outperforms PoolFormer-M36 using only 41% of its parameters. To demonstrate the applicability of SCHEME to larger models, we also present a comparison of the SCHEME version of the DaViT-Tiny using the UperNet framework [52]. While the DaViT-Tiny is already the best model of all in this section of the table, the use of the SCHEME mixer improves its performance by an additional **0.8** points.

Object Detection: Table 5 compares SCHEMEformer models to models of similar complexity on the COCO-17 object detection and instance segmentation benchmark, for both RetinaNet and Mask-RCNN detection heads. Again, the SCHEMEformer models outperform most other models of the same or smaller size. The only exception is the PoolFormer-S24, which slightly outperforms (0.1 points) the comparable SCHEMEformer-44-S24, for the RetinaNet head. However, with the stronger Mask R-CNN head, the SCHEMEformer-44-S24 beats the PoolFormer-S24 by 0.8 points. For the top performing models in the bottom third of each section of Table 5, SCHEME-DaViT-Tiny improves the box mAP of the top performing DaViT-Tiny by an additional **0.7%** and **0.9%**, for RetinaNet and MaskRCNN heads respectively, while maintaining a **comparable throughput**.

² With exception of the XCiT-T12/8

Table 5: COCO-17 Object Detection and Instance Segmentation. All backbones are pretrained on ImageNet-1K and use 1x learning schedule. AP^b and AP^m denote bounding box AP and mask AP, respectively. T denotes throughput (images/second).

RetinaNet 1x	#Par	T	AP	AP_{50}	AP_{75}	AP_S	AP_M	AP_L
PoolFormer-S12 [55]	21.7	13.1	36.2	56.2	38.2	20.8	39.1	48.0
ResNet-50 [20]	37.7	15.7	36.3	55.3	38.6	19.3	40.0	48.8
SCHEMEformer-44-e8-S12	21	6.1	38.3	58.0	40.4	21.0	41.4	52.3
PoolFormer-S24 [55]	31.1	8.9	38.9	59.7	41.3	23.3	42.1	51.8
ResNet-101 [20]	56.7	12.1	38.5	57.8	41.2	21.4	42.6	51.1
SCHEMEformer-44-e8-S24	31	3.5	38.8	58.7	41.2	22.5	41.5	53.5
DAT-T [51]	38	-	42.8	64.4	45.2	28.0	45.8	57.8
CrossFormer-S [48]	41	-	44.4	55.3	38.6	19.3	40.0	48.8
DaViT-Tiny [11]	39	8.2	44.0	65.6	47.3	29.6	47.9	57.3
SCHEME-DaViT-12-e8-Tiny	47	7.8	44.7	66.2	48.3	30.0	48.8	57.2
Mask R-CNN 1x	#Par	T	AP^b	AP_{50}^b	AP_{75}^b	AP^m	AP_{50}^m	AP_{75}^m
PoolFormer-S12 [55]	31.6	9.9	37.3	59.0	40.1	34.6	55.8	36.9
ResNet-50 [20]	44.2	15.4	38.0	58.6	41.4	34.4	55.1	36.7
SCHEMEformer-44-e8-S12	31	6.0	39.8	61.9	42.9	37.1	59.2	39.4
PoolFormer-S24 [55]	41.0	7.9	40.1	62.2	43.4	37.0	59.1	39.6
ResNet-101 [20]	63.2	12.1	40.4	61.1	44.2	36.4	57.7	38.8
SCHEMEformer-44-e8-S24	41	3.4	40.9	62.5	44.6	37.8	59.7	40.4
DAT-T [51]	48	-	44.4	67.6	48.5	40.4	64.2	43.1
CrossFormer-S [48]	50	-	45.4	68.0	49.7	41.4	64.8	44.6
DaViT-Tiny [11]	48	7.8	45.0	68.1	49.4	41.1	64.9	44.2
SCHEME-DaViT-12-e8-Tiny	57	7.4	45.9	68.3	50.2	41.5	65.4	44.3

4.2 Ablation Studies

In this section, we discuss ablations of the BD-MLP and CCA branches, alternative designs for the channel mixer, and the regularizing effect of CCA.

Contribution of BD-MLP and CCA branch: Table 6 shows an ablation of the contribution of the BD MLP and CCA branches to transformer performance. Starting from the Metaformer-PPAA-11-e2-S12, with expansion ratio $E = 2$ and dense MLP, we replace the channel mixer by SCHEME to obtain the SCHEMEformer-PPAA-44-e8-S12, which has $g_1 = g_2 = 4$ and $E = 8$, which maintains the number of parameters and FLOPs constant. The SCHEME model with only BD-MLP improves on the baseline by **0.2%**. The addition of the CCA branch provides an additional gain of **0.6%**, showing the gains of better feature clusters. Since CCA is not used at inference, its gains are *free* in terms of additional parameters/FLOPs.

Regularizing effect of CCA: Fig. 4a shows the evolution of the weight $1 - \alpha$ of the CCA branch in (6) during training. While initially large, it gradually decays to zero as training progresses. The figure shows that this holds for all network layers. Hence, CCA can be discarded at inference. Fig. 1 in supplementary plots the weights $1 - \alpha$ upon training convergence, for the family of SCHEMEformer-PPAA-44-e8 models, confirming that the weights are indeed very close to zero across all layers. Table 8 shows the impact of removing CCA at inference, for various backbones. While the number of FLOPs decreases, the top-1 accuracy changes very little (≈ 0.02 difference). Hence, there is no advantage in using CCA at inference. This is unlike training, where the use of CCA makes a non-negligible difference, as shown in Table 6.

Effect of large expansion ratios: The left of Figure 3 shows the effect of simultaneously increasing the expansion ratio E and adjusting groups to realize different models of similar size and complexity. All models are based on the Metaformer-PPAA-S12. For

Table 6: Ablation study of the contribution of BD-MLP and CCA branches to the overall performance for SCHEMEformer-PPAA-44-e8-S12 model. Baseline refers to Metaformer-PPAA-11-e2-S12.

Model	BDM	CCA	Acc (%)
Baseline			78.9
44-e8-S12	✓		79.1 (+0.2)
44-e8-S12	✓	✓	79.7 (+0.6)

Table 7: Ablation study of alternative designs for feature attention branch in SCHEME.

Module	#Par (M)	FLOPs (G)	Top-1 Acc (%)
Shuffle	11.83	1.77	79.1
SE	11.98	1.77	79.3
Conv	13.31	1.97	79.6
DyCCA	11.90	1.83	79.6
CCA	11.83	1.77	79.7

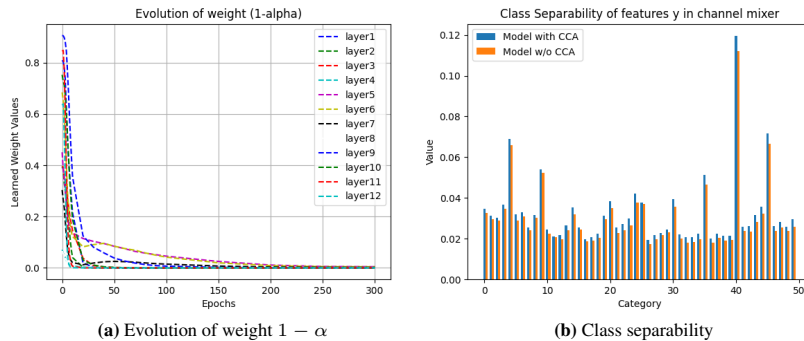


Fig. 4: Regularizing effect of CCA. (a) Evolution of weight $1 - \alpha$ across all layers for SCHEMEformer-PPAA-44-e8-S12 model. (b) Comparison of class separability of the features y of the SCHEME module, for 50 random classes on ImageNet-1K validation set, using SCHEMEformer-PPAA-44-e8-S12 model trained with and without CCA.

Table 8: Impact of removing CCA branch during inference.

Model	CCA Used	#Params (M)	FLOPs (G)	Top-1 Acc (%)
SCHEMEformer-PPAA-44-e8-S12	✓	11.83	2.16	79.74
SCHEMEformer-PPAA-44-e8-S12		11.83	1.77	79.72
SCHEMEformer-PPAA-12-e8-S24	✓	40.0	7.3	82.80
SCHEMEformer-PPAA-12-e8-S24		40.0	6.5	82.76
SCHEMEformer-PPAA-12-e8-S36	✓	58.8	10.8	84.00
SCHEMEformer-PPAA-12-e8-S36		58.8	9.6	83.95
SCHEME-CoatNet-44-e8-0	✓	17.80	3.83	80.70
SCHEME-CoatNet-44-e8-0		17.80	3.42	80.68
SCHEME-Swin-12-e8-T	✓	36.93	7.00	81.69
SCHEME-Swin-12-e8-T		36.93	5.89	81.69

fixed parameters/FLOPs, SCHEMEformer models achieve a gain of **1.0%** to **1.4%** over the baseline by increasing E from 1 to 4. The gains increase with larger expansions and saturate at larger FLOPs. This shows that higher internal feature dimensions are crucial for obtaining better accuracy with smaller ViT models.

Alternative designs of Channel Mixer:

We investigate whether alternative choices to the CCA branch could accomplish this goal more effectively. Table 7 compares models that replace CCA with other feature mixing operations: the channel shuffling operation of ShuffleNet [60], a squeeze and excitation [21] network (SENet), a single layer of convolution, and a dynamic version of CCA (DyCCA), where the weight α of (6) is predicted dynamically, using GCT attention [33]. The table shows that CCA obtains the best result. It is worth noting that while CCA computationally heavier than some of these alternatives, it is not needed during inference. We found this not to be true for the alternatives, which produce much more balanced weights α after training convergence, and cannot be discarded at inference without performance drop. We conjecture that, because the alternatives have learnable parameters, the network learns to use them to extract complementary features, which must be fused with those of the BD-MLP branch at inference. Thus, while small modules, the alternative designs incur a computational cost. CCA does not, achieving the best performance with no cost at inference.

Table 9: Ablation study on the formation of feature clusters in the BD-MLP branch of the SCHEME module.

Model	CCA	Group1 (%)	Group2 (%)	Group3 (%)	Group4 (%)	Ensemble (%)
SCHEMEformer-44-e8-S12		51.1	54.3	55.4	54.7	73.2
SCHEMEformer-s44-e8-S12	✓	47.6	50.0	49.2	55.1	73.8

Feature Clustering: We conjectured above that CCA helps training because it facilitates feature clustering into naturally independent groups that do not require inter-group communication. We tested this hypothesis by studying the intermediate feature vectors \mathbf{v}_l (obtained after max-pooling the features \mathbf{y} of (4)) extracted from four randomly selected layers l of two ImageNet pretrained models, trained with and without CCA respectively. We split the features into the 4 groups used in the model $\mathbf{v}_{l,g}, g \in \{1, \dots, 4\}$ and concatenated the features of all layers in the same group. This produced four vectors $\mathbf{u}_g = \text{concat}(\{\mathbf{v}_{l,g}\}_l)$ containing the features of each group g extracted throughout the network. A linear classifier was then learned over each vector \mathbf{u}_g . Table 16 shows the top-1 accuracy per feature group and model. To evaluate whether groups learn different class clusters, we also average the outputs from the four group classifiers to obtain the final accuracy. Without CCA, i.e. no group communication during training, the network produces feature groups that tend to be individually more predictive of the image class, but less predictive when combined. This suggests that there is some amount of redundancy between the features extracted by the different groups. By introducing inter-group communication, CCA enables the groups to learn more diverse sets of features, that complement each other.

Fig. 4b shows the class separability of the intermediate features \mathbf{y} of (4) of a randomly chosen layer of the SCHEMEformer-PPAA-44-e8-S12 model. Class separability was measured as in [35], with a final value obtained by averaging the class separability across all classes. The model trained with CCA has higher class separability than that without it. This confirms that CCA is helpful in forming feature clusters that increase class separability during training. Conversely, we tested if CCA is helpful when channel shuffling is inserted in between the two mixer MLP layers, which destroys the group structure. This variant of the SCHEMEformer-PPAA-44-e8-S12 model achieved an accuracy of 79.1% for both training with and without CCA. This shows that CCA is not helpful when feature groups are mixed. Similarly, CCA did not provide any gains when applied to the standard MLP branch with full feature mixing. These results suggest that CCA indeed helps to form the independent feature clusters needed to achieve the computational efficiency of channel groups without performance degradation.

5 Conclusion

In this work, we proposed the SCHEME module with sparse feature mixing for improving the performance of ViTs. This uses a weighted fusion of a BD-MLP branch, which abstracts existing MLPs with block diagonal structure, and a parameter-free CCA branch that helps to cluster features into groups during training. The CCA branch was shown to improve training but not be needed at inference. Experiments showed that it indeed improves the class separability of the internal feature representation of the BD-MLP branch, helping create feature clusters that are informative of the image class. The

standard MLP in transformer block is replaced with the SCHEME module to obtain a new family of SCHEMEformer models that were shown to improve performance for classification, detection, and segmentation, for fixed parameters and FLOPs with favorable latency. SCHEME is shown to be effective for various ViT architectures and was also shown to provide a flexible way to scale models, always outperforming models with smaller MLP expansion ratios having the same complexity.

References

1. Chen, B., Dao, T., Liang, K., Yang, J., Song, Z., Rudra, A., Ré, C.: Pixelated butterfly: Simple and efficient sparse training for neural network models. *International Conference on Learning Representations* (2021)
2. Chen, K., Wang, J., Pang, J., Cao, Y., Xiong, Y., Li, X., Sun, S., Feng, W., Liu, Z., Xu, J., Zhang, Z., Cheng, D., Zhu, C., Cheng, T., Zhao, Q., Li, B., Lu, X., Zhu, R., Wu, Y., Dai, J., Wang, J., Shi, J., Ouyang, W., Loy, C.C., Lin, D.: MMDetection: Open mmlab detection toolbox and benchmark. *arXiv preprint arXiv:1906.07155* (2019)
3. Chen, L.C., Papandreou, G., Kokkinos, I., Murphy, K., Yuille, A.L.: Deeplab: Semantic image segmentation with deep convolutional nets, atrous convolution, and fully connected crfs. *IEEE Transactions on Pattern Analysis and Machine Intelligence* **40**(4), 834–848 (2018). <https://doi.org/10.1109/TPAMI.2017.2699184>
4. Chen, Y., Dai, X., Chen, D., Liu, M., Dong, X., Yuan, L., Liu, Z.: Mobile-former: Bridging mobilenet and transformer. *ECCV* (2021)
5. Chollet, F.: Xception: Deep learning with depthwise separable convolutions. In: *2017 IEEE Conference on Computer Vision and Pattern Recognition (CVPR)*. pp. 1800–1807 (2017). <https://doi.org/10.1109/CVPR.2017.195>
6. Chu, X., Tian, Z., Zhang, B., Wang, X., Shen, C.: Conditional positional encodings for vision transformers. In: *The Eleventh International Conference on Learning Representations* (2023), <https://openreview.net/forum?id=3KWnuT-R1bh>
7. Contributors, M.: MMSegmentation: Openmmlab semantic segmentation toolbox and benchmark. <https://github.com/open-mmlab/mmssegmentation> (2020)
8. Dai, Z., Liu, H., Le, Q.V., Tan, M.: Coatnet: Marrying convolution and attention for all data sizes. *arXiv preprint arXiv:2106.04803* (2021)
9. Dao, T., Chen, B., Sohoni, N.S., Desai, A., Poli, M., Grogan, J., Liu, A., Rao, A., Rudra, A., Ré, C.: Monarch: Expressive structured matrices for efficient and accurate training. In: *International Conference on Machine Learning*. PMLR (2022)
10. Deng, J., Dong, W., Socher, R., Li, L.J., Li, K., Fei-Fei, L.: Imagenet: A large-scale hierarchical image database. In: *2009 IEEE Conference on Computer Vision and Pattern Recognition*. pp. 248–255 (2009). <https://doi.org/10.1109/CVPR.2009.5206848>
11. Ding, M., Xiao, B., Codella, N., Luo, P., Wang, J., Yuan, L.: Davit: Dual attention vision transformers. In: *Computer Vision–ECCV 2022: 17th European Conference, Tel Aviv, Israel, October 23–27, 2022, Proceedings, Part XXIV*. pp. 74–92. Springer (2022)
12. Dong, X., Bao, J., Chen, D., Zhang, W., Yu, N., Yuan, L., Chen, D., Guo, B.: Cswin transformer: A general vision transformer backbone with cross-shaped windows (2021)
13. Dong, Y., Cordonnier, J.B., Loukas, A.: Attention is not all you need, pure attention loses rank doubly exponentially with depth. *ICML* (2021), <https://arxiv.org/abs/2103.03404>
14. Dosovitskiy, A., Beyer, L., Kolesnikov, A., Weissenborn, D., Zhai, X., Unterthiner, T., Dehghani, M., Minderer, M., Heigold, G., Gelly, S., Uszkoreit, J., Houlsby, N.: An image is

- worth 16x16 words: Transformers for image recognition at scale. In: International Conference on Learning Representations (2021), <https://openreview.net/forum?id=YicbFdNTTy>
15. El-Nouby, A., Touvron, H., Caron, M., Bojanowski, P., Douze, M., Joulin, A., Laptev, I., Neverova, N., Synnaeve, G., Verbeek, J., et al.: Xcit: Cross-covariance image transformers. arXiv preprint arXiv:2106.09681 (2021)
 16. Fedus, W., Zoph, B., Shazeer, N.: Switch transformers: Scaling to trillion parameter models with simple and efficient sparsity. *Journal of Machine Learning Research* (2022)
 17. Fu, D.Y., Arora, S., Grogan, J., Johnson, I., Eyuboglu, S., Thomas, A.W., Spector, B., Poli, M., Rudra, A., Ré, C.: Monarch mixer: A simple sub-quadratic gemm-based architecture. In: *Advances in Neural Information Processing Systems* (2023)
 18. Graham, B., El-Nouby, A., Touvron, H., Stock, P., Joulin, A., Jegou, H., Douze, M.: Levit: A vision transformer in convnet's clothing for faster inference. In: *Proceedings of the IEEE/CVF International Conference on Computer Vision (ICCV)*. pp. 12259–12269 (October 2021)
 19. He, K., Gkioxari, G., Dollár, P., Girshick, R.: Mask r-cnn. In: *2017 IEEE International Conference on Computer Vision (ICCV)*. pp. 2980–2988 (2017). <https://doi.org/10.1109/ICCV.2017.322>
 20. He, K., Zhang, X., Ren, S., Sun, J.: Deep residual learning for image recognition. *2016 IEEE Conference on Computer Vision and Pattern Recognition (CVPR)* pp. 770–778 (2015)
 21. Hu, J., Shen, L., Sun, G.: Squeeze-and-excitation networks. In: *IEEE Conference on Computer Vision and Pattern Recognition* (2018)
 22. Kirillov, A., Girshick, R., He, K., Dollár, P.: Panoptic feature pyramid networks. In: *2019 IEEE/CVF Conference on Computer Vision and Pattern Recognition (CVPR)*. pp. 6392–6401. IEEE Computer Society, Los Alamitos, CA, USA (jun 2019). <https://doi.org/10.1109/CVPR.2019.00656>, <https://doi.ieeecomputersociety.org/10.1109/CVPR.2019.00656>
 23. Krizhevsky, A., Sutskever, I., Hinton, G.E.: Imagenet classification with deep convolutional neural networks. In: Pereira, F., Burges, C., Bottou, L., Weinberger, K. (eds.) *Advances in Neural Information Processing Systems*. vol. 25. Curran Associates, Inc. (2012), <https://proceedings.neurips.cc/paper/2012/file/c399862d3b9d6b76c8436e924a68c45b-Paper.pdf>
 24. Li, Y., Yuan, G., Wen, Y., Hu, J., Evangelidis, G., Tulyakov, S., Wang, Y., Ren, J.: Efficientformer: Vision transformers at mobilenet speed. *Neurips* (2022)
 25. Li, Y., Zhang, K., Cao, J., Timofte, R., Van Gool, L.: Localvit: Bringing locality to vision transformers. arXiv preprint arXiv:2104.05707 (2021)
 26. Lin, T.Y., Goyal, P., Girshick, R., He, K., Dollár, P.: Focal loss for dense object detection. *ICCV* (2017)
 27. Lin, T.Y., Maire, M., Belongie, S., Bourdev, L., Girshick, R., Hays, J., Perona, P., Ramanan, D., Zitnick, C.L., Dollár, P.: Microsoft coco: Common objects in context. In: *ECCV*. pp. 740–755 (2014). <https://doi.org/10.48550/ARXIV.1405.0312>
 28. Liu, H., Dai, Z., So, D.R., Le, Q.V.: Pay attention to mlps (2021). <https://doi.org/10.48550/ARXIV.2105.08050>, <https://arxiv.org/abs/2105.08050>
 29. Liu, Y., Zhang, Y., Wang, Y., Hou, F., Yuan, J., Tian, J., Zhang, Y., Shi, Z., Fan, J., He, Z.: A survey of visual transformers (2021). <https://doi.org/10.48550/ARXIV.2111.06091>, <https://arxiv.org/abs/2111.06091>
 30. Liu, Z., Lin, Y., Cao, Y., Hu, H., Wei, Y., Zhang, Z., Lin, S., Guo, B.: Swin transformer: Hierarchical vision transformer using shifted windows. In: *Proceedings of the IEEE/CVF International Conference on Computer Vision (ICCV)* (2021)

31. Parmar, N.J., Vaswani, A., Uszkoreit, J., Kaiser, L., Shazeer, N., Ku, A., Tran, D.: Image transformer. In: International Conference on Machine Learning (ICML) (2018), <http://proceedings.mlr.press/v80/parmar18a.html>
32. Ramachandran, P., Parmar, N., Vaswani, A., Bello, I., Levskaya, A., Shlens, J.: Stand-alone self-attention in vision models. In: Wallach, H., Larochelle, H., Beygelzimer, A., d'Alché-Buc, F., Fox, E., Garnett, R. (eds.) *Advances in Neural Information Processing Systems*. vol. 32. Curran Associates, Inc. (2019), <https://proceedings.neurips.cc/paper/2019/file/3416a75f4cea9109507cacd8e2f2aefc-Paper.pdf>
33. Ruan, D., Wang, D., Zheng, Y., Zheng, N., Zheng, M.: Gaussian context transformer. In: *Proceedings of the IEEE/CVF Conference on Computer Vision and Pattern Recognition (CVPR)*. pp. 15129–15138 (June 2021)
34. Sandler, M., Howard, A., Zhu, M., Zhmoginov, A., Chen, L.C.: Mobilenetv2: Inverted residuals and linear bottlenecks. *CVPR* (2018)
35. Schilling, A., Maier, A., Gerum, R., Metzner, C., Krauss, P.: Quantifying the separability of data classes in neural networks. *Neural Networks* **139**, 278–293 (2021). <https://doi.org/https://doi.org/10.1016/j.neunet.2021.03.035>, <https://www.sciencedirect.com/science/article/pii/S0893608021001234>
36. Shazeer, N., Mirhoseini, A., Maziarz, K., Davis, A., Le, Q., Hinton, G., Dean, J.: Outrageously large neural networks: The sparsely-gated mixture-of-experts layer. In: *International Conference on Learning Representations* (2017), <https://openreview.net/forum?id=BlckMDqlg>
37. Srinivas, A., Lin, T.Y., Parmar, N., Shlens, J., Abbeel, P., Vaswani, A.: Bottleneck transformers for visual recognition. In: *CVPR* (2021). <https://doi.org/10.48550/ARXIV.2101.11605>, <https://arxiv.org/abs/2101.11605>
38. Tang, S., Zhang, J., Zhu, S., Tan, P.: Quadtree attention for vision transformers. *ICLR* (2022)
39. Touvron, H., Cord, M., Douze, M., Massa, F., Sablayrolles, A., Jégou, H.: Training data-efficient image transformers and distillation through attention. In: *International Conference on Machine Learning*. vol. 139, pp. 10347–10357 (July 2021)
40. Touvron, H., Cord, M., El-Nouby, A., Verbeek, J., Jégou, H.: Three things everyone should know about vision transformers. *ECCV* (2022)
41. Touvron, H., Cord, M., Jégou, H.: Deit iii: Revenge of the vit. *ECCV* (2022)
42. Touvron, H., Cord, M., Sablayrolles, A., Synnaeve, G., Jégou, H.: Going deeper with image transformers. In: *Proceedings of the IEEE/CVF International Conference on Computer Vision (ICCV)*. pp. 32–42 (October 2021)
43. Tu, Z., Talebi, H., Zhang, H., Yang, F., Milanfar, P., Bovik, A., Li, Y.: Maxvit: Multi-axis vision transformer. *ECCV* (2022)
44. Vaswani, A., Ramachandran, P., Srinivas, A., Parmar, N., Hechtman, B., Shlens, J.: Scaling local self-attention for parameter efficient visual backbones. In: *CVPR* (2021)
45. Vaswani, A., Shazeer, N., Parmar, N., Uszkoreit, J., Jones, L., Gomez, A.N., Kaiser, L.u., Polosukhin, I.: Attention is all you need. In: Guyon, I., Luxburg, U.V., Bengio, S., Wallach, H., Fergus, R., Vishwanathan, S., Garnett, R. (eds.) *Advances in Neural Information Processing Systems*. vol. 30. Curran Associates, Inc. (2017), <https://proceedings.neurips.cc/paper/2017/file/3f5ee243547dee91fbd053c1c4a845aa-Paper.pdf>
46. Wang, W., Xie, E., Li, X., Fan, D.P., Song, K., Liang, D., Lu, T., Luo, P., Shao, L.: Pyramid vision transformer: A versatile backbone for dense prediction without convolutions. In: *Proceedings of the IEEE/CVF International Conference on Computer Vision*. pp. 568–578 (2021)
47. Wang, W., Xie, E., Li, X., Fan, D.P., Song, K., Liang, D., Lu, T., Luo, P., Shao, L.: PVT v2: Improved baselines with pyramid vision transformer. *Computational Visual Media* (2022)

48. Wang, W., Yao, L., Chen, L., Lin, B., Cai, D., He, X., Liu, W.: Crossformer: A versatile vision transformer hinging on cross-scale attention. In: International Conference on Learning Representations, ICLR (2022), https://openreview.net/forum?id=_PHymLIxuI
49. Wu, H., Xiao, B., Codella, N., Liu, M., Dai, X., Yuan, L., Zhang, L.: Cvt: Introducing convolutions to vision transformers. IEEE/CVF International Conference on Computer Vision (ICCV) (2021)
50. Wu, K., Peng, H., Chen, M., Fu, J., Chao, H.: Rethinking and improving relative position encoding for vision transformer. In: 2021 IEEE/CVF International Conference on Computer Vision (ICCV). pp. 10013–10021. IEEE Computer Society, Los Alamitos, CA, USA (oct 2021). <https://doi.org/10.1109/ICCV48922.2021.00988>, <https://doi.ieeecomputersociety.org/10.1109/ICCV48922.2021.00988>
51. Xia, Z., Pan, X., Song, S., Li, L.E., Huang, G.: Vision transformer with deformable attention. In: Proceedings of the IEEE/CVF Conference on Computer Vision and Pattern Recognition (CVPR). pp. 4794–4803 (June 2022)
52. Xiao, T., Liu, Y., Zhou, B., Jiang, Y., Sun, J.: Unified perceptual parsing for scene understanding. In: European Conference on Computer Vision. Springer (2018)
53. Xie, S., Girshick, R., Dollar, P., Tu, Z., He, K.: Aggregated residual transformations for deep neural networks. In: 2017 IEEE Conference on Computer Vision and Pattern Recognition (CVPR). pp. 5987–5995 (07 2017). <https://doi.org/10.1109/CVPR.2017.634>
54. Yang, J., Li, C., Zhang, P., Dai, X., Xiao, B., Yuan, L., Gao, J.: Focal self-attention for local-global interactions in vision transformers (2021)
55. Yu, W., Luo, M., Zhou, P., Si, C., Zhou, Y., Wang, X., Feng, J., Yan, S.: Metaformer is actually what you need for vision. In: Proceedings of the IEEE/CVF Conference on Computer Vision and Pattern Recognition. pp. 10819–10829 (2022)
56. Yuan, K., Guo, S., Liu, Z., Zhou, A., Yu, F., Wu, W.: Incorporating convolution designs into visual transformers (2021). <https://doi.org/10.48550/ARXIV.2103.11816>, <https://arxiv.org/abs/2103.11816>
57. Yuan, L., Chen, Y., Wang, T., Yu, W., Shi, Y., Jiang, Z.H., Tay, F.E., Feng, J., Yan, S.: Tokens-to-token vit: Training vision transformers from scratch on imagenet. In: Proceedings of the IEEE/CVF International Conference on Computer Vision (ICCV). pp. 558–567 (October 2021)
58. Zhang, P., Dai, X., Yang, J., Xiao, B., Yuan, L., Zhang, L., Gao, J.: Multi-scale vision longformer: A new vision transformer for high-resolution image encoding. ICCV 2021 (2021)
59. Zhang, P., Dai, X., Yang, J., Xiao, B., Yuan, L., Zhang, L., Gao, J.: Multi-scale vision longformer: A new vision transformer for high-resolution image encoding. In: Proceedings of the IEEE/CVF International Conference on Computer Vision (ICCV). pp. 2998–3008 (October 2021)
60. Zhang, X., Zhou, X., Lin, M., Sun, J.: Shufflenet: An extremely efficient convolutional neural network for mobile devices. In: 2018 IEEE Conference on Computer Vision and Pattern Recognition (CVPR). pp. 6848–6856 (06 2018). <https://doi.org/10.1109/CVPR.2018.00716>
61. Zhou, B., Zhao, H., Puig, X., Fidler, S., Barriuso, A., Torralba, A.: Scene parsing through ade20k dataset. In: 2017 IEEE Conference on Computer Vision and Pattern Recognition (CVPR). pp. 5122–5130 (2017). <https://doi.org/10.1109/CVPR.2017.544>

Appendix

A Implementation Details

A.1 Hyperparameter Settings

Table 10 shows the detailed hyperparameter settings of the family of SCHEMEformer models reported in the main paper.

Table 10: Hyperparameter Settings for the family of SCHEMEformer models trained on ImageNet-1K dataset.

Model	SCHEMEformer-PPAA-44-e8			SCHEMEformer-PPAA-12-e8			SCHEME-CAformer	
	S12	S24	S36	S12	S24	S36	44-e8-S18	12-e8-S12
Peak drop rate of stoch. depth d_r	0.1	0.2	0.4	0.1	0.2	0.4	0.15	0.15
LayerScale initialization ϵ	10^{-5}	10^{-5}	10^{-6}	10^{-5}	10^{-5}	10^{-6}	10^{-5}	10^{-5}
Data augmentation	AutoAugment							
Repeated Augmentation	off							
Input resolution	224							
Epochs	300							
Hidden dropout	0							
GELU dropout	0							
Classification dropout	0							
Random erasing prob	0.25							
EMA decay	0							
Cutmix α	1.0							
Mixup α	0.8							
Cutmix-Mixup switch prob	0.5							
Label smoothing	0.1							
Batch size used in the paper	1024							
Learning rate decay	cosine							
Weight decay	0.05							
Gradient clipping	None							
Warmup epochs	5						20	
Relation between peak learning rate and batch size	$\text{lr} = \frac{\text{batch size}}{1024} \times e^{-3}$						$\text{lr} = \frac{\text{batch size}}{1024} \times 8 \times e^{-3}$	
Optimizer	AdamW							
Adam ϵ	$1e^{-8}$							
Adam (β_1, β_2)	(0.9, 0.999)							

B Ablation Studies

B.1 Plot of the learned $1 - \alpha$ weights in the SCHEME module for SCHEMEformer models

The learned weights $1 - \alpha$ for the family of SCHEMEformer models is shown in Fig. 5. Interestingly, the learned weights coarsely approximate the shape of a gaussian distribution. The learned weights reach a peak value in the middle layers of the network and drop to zero for all the other layers. The middle of the network typically correspond to the initial few layers of the third stage of the model that contains the maximum number of transformer blocks for all the models shown in Fig. 5. We conjecture that the weights for these layers have not fully converged and that feature mixing can still be useful for these layers and so training for more epochs will allow the $1 - \alpha$ weights of these layers to converge to zero. To test this hypothesis, we trained the SCHEMEformer-PPAA-12-e8-S12 model for an additional 200 epochs beyond the standard 300 epochs

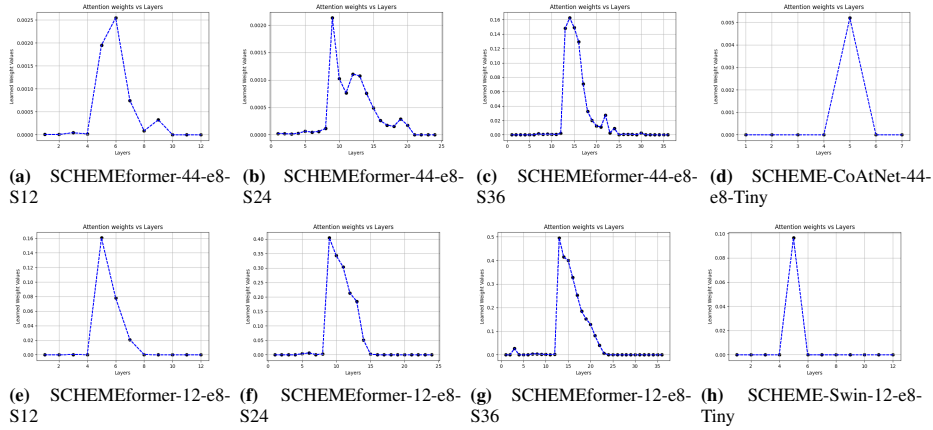


Fig. 5: Plot of the learned weight ($1-\alpha$) values across different layers of a network for the family of SCHEMEformer models. The weights reach a peak value near the middle of the network. We demonstrate that these peak weights are not yet converged and training the network for more epochs decays these weights to zero while also improving the accuracy. For example, training the SCHEMEformer-PPAA-12-e8-S12 model for 200 additional epochs reduced the weight norm of the vector of $1-\alpha$ weights from 0.18 to 0.05 showing that these weights gradually approach zero as the training progresses while improving the accuracy further by 0.4%.

Table 11: Training Overhead of CCA. CCA adds only a small overhead in GPU memory and training time.

Model	CCA	#Par (M) ↓	Train FLOPs (G) ↓	Val Acc (%) ↑	GPU Mem. (G) ↓	Train Throughput (iters/s) ↑
SCHEMEformer-PPAA-44-e8-S12		11.8	1.77	79.1	8	215
SCHEMEformer-PPAA-44-e8-S12	✓	11.8	2.16	79.7	9	180

Table 12: Ablation study of longer training for SCHEMEformer-PPAA-44-e8-S12.

Model	#Params (M)	FLOPs (G)	Throughput (img/s)	300-Acc (%)	500-Acc (%)
Metaformer-11-e2-S12 (Baseline)	11.8	1.77	133	78.9	79.6
SCHEMEformer-PPAA-44-e8-S12	11.8	1.77	133	79.7	80.1

and observed that the peak value of the $1-\alpha$ weights decreased further by 0.11 as compared to the model trained for 300 epochs and the accuracy improved by **0.4%**. The weight norm (of all layers) decreased from 0.18 for 300 epoch model to 0.05 for 500 epoch model. This confirms our hypothesis and training SCHEMEformer models for larger epochs can further improve the accuracy.

B.2 Training Overhead of CCA

Table 11 compares the training GPU memory and throughput for SCHEME mixer with and without using CCA. CCA improves the accuracy by 0.6% with only a slight increase in the GPU memory (+12.5%) and training time (+16.7%). Further, CCA is not needed during inference thereby providing gains for "free" without additional computational cost at inference.

Table 13: Ablation study of removing CCA for COCO-17 Object Detection and Instance Segmentation. Removing CCA at inference does not impact the AP values as they are identical to the model using CCA at inference. AP^b and AP^m denote bounding box AP and mask AP, respectively. Backbone models denote SCHEMEformer-PPAA-44-e8- variants.

Backbone	CCA Used	RetinaNet 1x							Mask R-CNN 1x							CCA	Semantic FPN		
		#P	AP	AP_{50}^b	AP_{75}^b	AP_S^b	AP_M	AP_L	#P	AP^b	AP_{50}^b	AP_{75}^b	AP^m	AP_{50}^m	AP_{75}^m		#Par	FLOPs	mIoU (%)
S12	✓	21	38.3	58.0	40.4	21.0	41.4	52.3	31	39.8	61.9	42.9	24.1	53.0	42.3	✓	15.5	36.4	40.9
S12		21	38.3	58.0	40.4	21.0	41.4	52.3	31	39.8	61.9	42.9	24.1	53.0	42.3		15.5	34.3	40.9
S24	✓	31	38.8	58.7	41.2	22.5	41.5	53.5	41	40.9	62.5	44.6	24.6	55.6	43.8	✓	24.8	49.8	42.5
S24		31	38.8	58.7	41.2	22.5	41.5	53.5	41	40.9	62.5	44.6	24.6	55.6	43.8		24.8	45.7	42.5

Table 15: Ablation study on the effect of larger expansion ratios in BD-MLP block of SCHEME on ImageNet-1K validation dataset.

Model	#Par (M)	FLOPs (G)	Top-1 Acc (%)
Metaformer-PPAA-11-e1-S12	9.6	1.37	76.0
SCHEMEformer-PPAA-22-e2-S12	9.6	1.37	77.0
SCHEMEformer-PPAA-44-e4-S12	9.6	1.37	77.4
SCHEMEformer-PPAA-66-e6-S12	10.0	1.45	77.9
Metaformer-PPAA-11-e2-S12	11.8	1.77	78.9
SCHEMEformer-PPAA-22-e4-S12	11.8	1.77	79.4
SCHEMEformer-PPAA-44-e8-S12	11.8	1.77	79.7
SCHEMEformer-PPAA-33-e6-S12	12.5	1.87	79.8
SCHEMEformer-PPAA-22-e6-S12	14.1	2.16	80.4
Metaformer-PPAA-11-e4-S12	16.5	2.56	81.0
SCHEMEformer-PPAA-22-e8-S12	16.5	2.56	81.1
SCHEMEformer-PPAA-44-e16-S12	16.5	2.56	81.2

B.3 Training for longer epochs

Table 12 shows the comparison of training for longer epochs for SCHEMEformer with the baseline Metaformer model. We train for an additional 200 epochs from the standard 300 epochs. SCHEMEformer-PPAA-44-e8-S12 trained for 300 epochs even outperforms the baseline model trained for 500 epochs. On continuing the training from 300 to 500 epochs, SCHEMEformer continues to improve the performance without saturation suggesting that it is beneficial to train with CCA for longer epochs. 300 to 500 epochs is a much larger increase of training time (67%) than the 16.7% increase in training time required by SCHEME mixer (see Table 11).

B.4 Impact of removing CCA at inference for Object Detection and Semantic Segmentation

Table 13 and 14 show the results of removing CCA at inference for object detection and semantic segmentation models, respectively. For both tasks, the results are identical to the model using CCA showing that the CCA also generalizes to downstream tasks.

B.5 CCA

In the main paper, feature groups across different layers of the model was used to demonstrate the learning of feature clusters by CCA. Here, the feature from the final layer of the model is only considered. Table 16 shows the top-1 accuracy per feature group and model. The average of the outputs from the four group classifiers is reported in the final column of the table. The effect is more pronounced when using a single

Table 16: Ablation study on the formation of feature clusters in the BD-MLP branch of the SCHEME module. We train a linear classifier on top of the four feature groups extracted from the final MLP mixer of the transformer block of the network. The model trained with CCA forms feature clusters that learn diverse and complementary set of features that can obtain 1% higher validation accuracy than the model trained without CCA.

Model	CCA	Group1 (%)	Group2 (%)	Group3 (%)	Group4 (%)	Ensemble (%)
SCHEMEformer-44-e8-S12		29.63	37.59	37.57	35.89	73.95
SCHEMEformer-44-e8-S12	✓	27.89	37.64	30.02	37.67	75.04

layer feature with **+1.09%** accuracy difference between the model with and without CCA. This further reinforces that by introducing inter-group communication, CCA enables the groups to learn more diverse sets of features, that complement each other.

B.6 Larger expansion ratios

Table 15 shows additional results of using larger expansion ratios with SCHEME mixer (illustrated in Fig. 3 of the main paper) for the same number of parameters and FLOPs using the Metaformer-PPAA-S12 baseline model. We observe that SCHEMEformer-PPAA consistently outperforms the baseline for larger expansions ratios with larger gains at lower FLOPs. The performance saturates as the model size and FLOPs increases.

C Qualitative Analysis: Grad-CAM Visualization

Fig. 6 shows the results of class activation maps for SCHEMEformer-PPAA-44-e8-S12 model for a few examples from the validation set of ImageNet-1K dataset. The stronger heatmap responses around the salient features of an object (e.g., body of a bird, cat) shows that the model ignores the background and attends to more discriminative spatial regions. Fig. 6 also shows the qualitative comparison with a few existing methods such as ResNet-50, DeiT-S, Poolformer etc. of similar complexity. It demonstrates that SCHEMEformer-PPAA-44-e8-S12 attends to the complete object class and less spurious features showing that it is better than the competing methods.

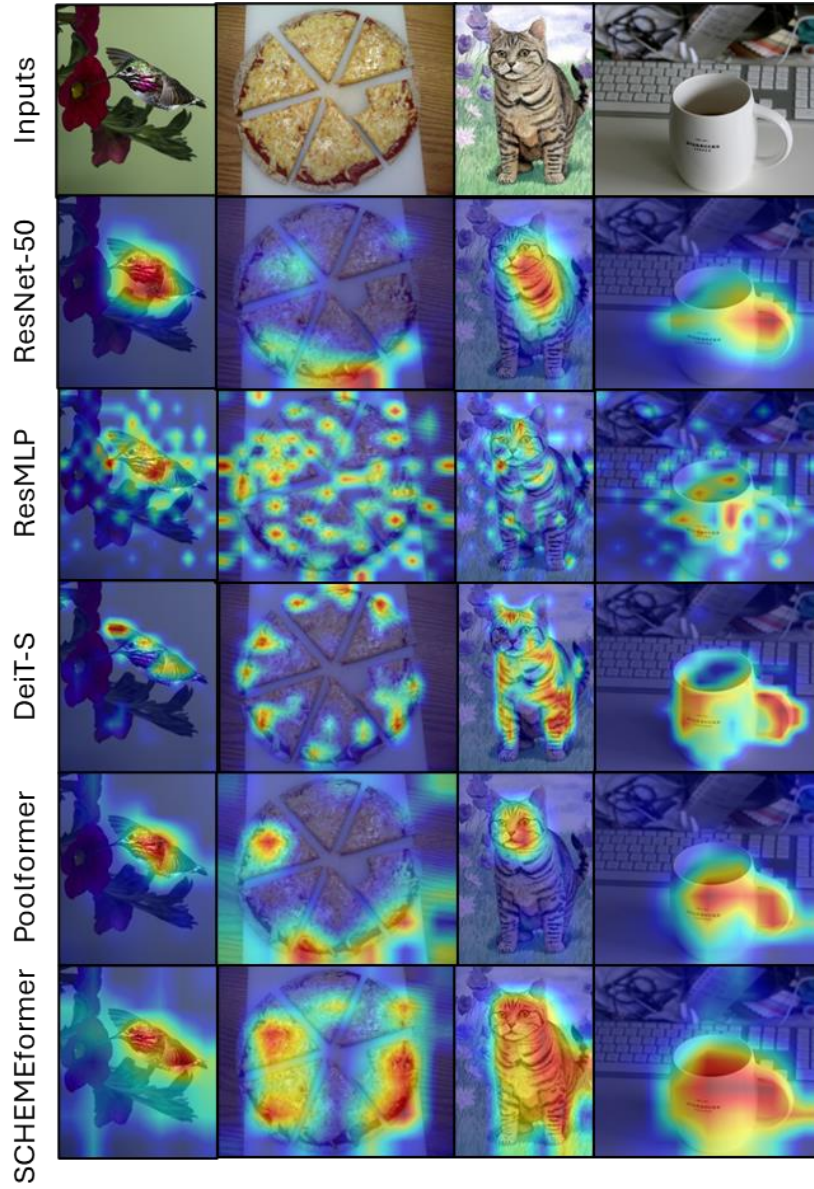


Fig. 6: GRAD-CAM visualization for a few validation samples on ImageNet-1K dataset for SCHEMEformer-PPAA-44-e8-S12 model and comparison with other competing methods.